Mathematics

https://www.aimspress.com/journal/Math

AIMS Mathematics, 11(7): 20773–20801.
DOI: 10.3934/math.2026844
Received: 11 May 2026
Revised: 29 June 2026
Accepted: 08 July 2026
Published: 14 July 2026

Research article

Construction of two-direction scaling functions on generalized elliptic helical curves

Gang Wang* **and Zhihui Zhang**

School of Mathematical Sciences, Xinjiang Normal University, Urumqi, Xinjiang 830017, China

* **Correspondence:** Email: angelayy@sina.com.

Abstract: Based on an arc length-preserving projection, this paper investigates two-direction scaling functions on generalized elliptic helical curves. The spatial trace of the parametrization is distinguished from its parametrized carrier, so repeated spatial points caused by periodicity or self-intersection remain distinct when their parameter values differ. Under the stated parameter restrictions, the speed has a positive uniform lower bound; consequently, on the global carrier with parameter interval $I = \mathbb{R}$, the oriented arc length coordinate is a homeomorphism onto $\mathbb{R}$. This yields a nonempty global setting in which the real line two-direction multiresolution structure can be transferred to the curve without boundary truncation. Through the induced unitary identification between $L^2(\mathbb{R})$ and the carrier space, the two-direction refinement equations and the scaling and wavelet coefficient sequences are transported in a consistent arc length formulation. Riesz basis and orthogonality properties are preserved whenever the corresponding real line families possess them. The mask matrix spectral condition is treated separately from cascade convergence, L^2-stability, continuity, the Riesz basis property, and orthogonality, and a necessary Hermitian paraunitary mask condition is derived for orthogonal two-direction scaling functions. Under the corresponding real line approximation assumptions, approximation order estimates are likewise transported to the carrier. For numerical verification, a bounded injective spatial segment is considered independently, and the arc length map is approximated by an explicit Euler scheme. Finally, two algebraically checked symbolic mask examples, together with the numerical projection experiment, illustrate the discretization procedure and the relevant algebraic mask conditions.

Keywords: arc length-preserving projection; Euler discretization; generalized elliptic-helical curve; two-direction scaling function; wavelet analysis
Mathematics Subject Classification: 42C40, 42C15, 65D30

1. Introduction

Wavelet theory provides an effective framework for dealing with nonstationary data because it can describe local time domain features and analyze signals at multiple scales [1]. Due to these advantages, wavelet analysis has been used in a wide range of areas, such as signal processing [1], wavelet analysis on smooth surfaces [2], biometric recognition [3], and financial data analysis [4–6].

Group-theoretic and representation-theoretic methods have been used to construct spatiotemporal continuous wavelet transforms for signal and motion analysis [7, 8]. Another useful approach is to transfer wavelet constructions between Euclidean domains and manifolds or parametrized curves through suitable geometric projections and inverse projections [9–14].

Related work and contribution

Earlier curve-based wavelet studies include applications to regression trend curves in financial data models and theoretical constructions for signals indexed by smooth or helical curves [5, 6, 13, 14]. These works motivate the mathematical question considered here: how a real line two-direction refinement structure changes when the independent variable is replaced by arc length along a parametrized space curve. Trajectories, filamentary data, and other curve-supported signals are possible future settings, but they are not tested in this article. Accordingly, no application-specific accuracy, reconstruction, or performance claim is made here; the contribution is limited to the curve coordinate theory and the numerical verification of the arc length discretization.

In recent years, the theory of wavelet analysis on curves has been further developed. Zhou systematically studied wavelet transforms on generalized helical curves, constructed locally continuous wavelets by means of tangential projection, derived the corresponding reconstruction formula, and further implemented discrete wavelet lifting using an arc length-preserving projection [13]. These studies provide theoretical support for wavelet analysis on generalized helical space curves and motivate further investigation of multiscale methods for signals distributed along such curves, including the curve-based construction developed in this paper.

As modulated extensions of the circular transverse trajectory in Eq (2.1), the generalized elliptic helical curves considered here provide a useful geometric setting for investigating functions and multiscale constructions on parametrized space curves. However, current research is still in the transitional stage from the general theory of helical curves to the special case of generalized elliptic helical curves. In particular, Yang and Li [15] introduced and systematically studied two-direction refinable functions and two-direction wavelets, including their properties and construction procedures. Nevertheless, the transfer of real line two-direction wavelet structures to generalized elliptic helical curves has not yet been fully developed. This motivates the present work.

The central idea of this paper is to use an arc length-preserving projection as a bridge between the real line and generalized elliptic helical curves. Through this projection, two-direction scaling functions and wavelets originally defined on the real line can be transferred to the curve setting without changing the essential multiresolution structure. In this way, the real line two-direction refinement relations induce corresponding curve-based refinement equations on generalized elliptic helical curves. This provides a systematic method for constructing two-direction scaling functions directly associated with generalized elliptic helical curves.

Related developments in non-Euclidean multiscale analysis include diffusion wavelets on manifolds and graphs [16], spectral graph wavelets [17], graph signal processing [18], scattering transforms [19, 20], graph convolutional methods [21–23], and geometric deep learning frameworks [24]. These works show the importance of localized multiscale representations adapted to geometric data. However, they do not address the transfer of two-direction refinement equations to generalized elliptic helical curves by means of an arc length-preserving projection. Compared with existing wavelet constructions on smooth curves and generalized helical curves, the present work focuses specifically on the curve-based formulation of two-direction refinement structures, including coefficient correspondence; a clear separation of the spectral, convergence, stability, and orthogonality assumptions; Hermitian orthogonality criteria; and approximation order properties.

The relation to earlier literature is as follows. References [13, 14] established one-direction curve wavelet constructions using a length coordinate, whereas [15] developed two-direction refinable functions on the real line. The arc length map and the induced Hilbert space isometry used below are therefore inherited tools, not new projection results. The contribution claimed in this paper is the compatibility analysis obtained after these two ingredients are combined: The two-direction refinement equations, coefficient correspondence, spectral condition, necessary Hermitian orthogonality test, and approximation estimate are written in one consistent arc length notation for the generalized elliptic helical setting. No claim is made that the underlying length-preserving projection or the one-direction transport principle originate here.

In this paper, the Euler discretization method for arc length-preserving projection is employed to investigate two-direction scaling functions on generalized elliptic helical curves. The projection not only establishes the connection between functions on the real line and functions on the curve but also allows the refinement coefficients; the distinction among spectral, convergence, stability, and orthogonality assumptions; Hermitian orthogonality conditions; and approximation order properties of real line two-direction wavelets to be reformulated in the curve-based setting.

The main contributions are summarized below. First, an arc length-preserving projection model for generalized elliptic helical curves is combined with two-direction refinement relations, which allows two-direction scaling functions to be transferred from the real line to generalized elliptic helical curves. Second, using this projection, a two-direction multiresolution structure and the associated two-direction refinement relations are developed on generalized elliptic helical curves. Third, the relationship between the real line refinement coefficients and their curve-based counterparts is established. Finally, necessary Hermitian orthogonality conditions; a clear separation of the spectral, convergence, stability, and orthogonality assumptions; approximation-order transport results; and explicit symbolic mask examples are provided for curve-based two-direction scaling functions.

The organization is summarized below. Section 2 introduces the spatial trace and parametrized carrier of a generalized elliptic helical curve, proves the global arc length coordinate property on the carrier, presents its Euler approximation, and recalls the required real line two-direction preliminaries. Section 3 formulates the curve-based multiresolution and refinement relations on the global carrier. Section 4 treats solvability, Hermitian orthogonality, a necessary Hermitian matrix mask condition, and approximation order. Section 5 reports the reproducible Euler test on a bounded injective spatial segment and gives two checked symbolic examples.

2. Preliminaries

This section presents generalized elliptic helical curves together with their discretized arc length-preserving projections followed by a brief review of the basic theory for two-direction wavelet analysis.

2.1. Generalized elliptic helical curves and their discrete arc length-preserving projections

Previous studies have investigated trajectories generated by superposed circular motions. Consider a particle that undergoes circular motion about a fixed axis while simultaneously undergoing a second circular modulation. The resulting trajectory is a periodic modulated space curve rather than the standard circular helix with a linear axial coordinate. We use the following circular transverse case only as a precursor to the generalized elliptic helical model:

$$\vec{r}(t) = ((a + v_0 \cos(\Omega t))\cos(t), (a + v_0 \cos(\Omega t))\sin(t), v_0 \sin(\Omega t)). \tag{2.1}$$

Here, the condition $|v_0| < a$ is imposed; a and v_0 represent the corresponding radii of the two rotations, and Ω denotes the rotation rate.

Replacing the equal transverse base radii in (2.1) by two generally unequal values a and b gives the generalized elliptic helical trajectory used below.

Definition 2.1 (Generalized elliptic helical curve; cf. [13, 25])**.** Let $I \subseteq \mathbb{R}$ be an interval, and fix a reference parameter $t_* \in I$. The curve under study is the regular parametrized curve $\gamma : I \to \mathbb{R}^3$ given by

$$\gamma(t) = ((a + v_0 \cos(\Omega t))\cos t, (b + v_0 \cos(\Omega t))\sin t, v_0 \sin(\Omega t)). \tag{2.2}$$

Here, $a > 0$, $b > 0$, $|v_0| < \min\{a, b\}$, and $\Omega \neq 0$. Because the third coordinate in (2.2) is periodic rather than monotone, the curve is not the standard elliptic helix on a vertical elliptic cylinder. It is a modulated generalized elliptic helical curve. The inequalities keep both transverse radii positive. Differentiation gives

$$\begin{aligned}\gamma'(t) = (&-v_0\Omega \sin(\Omega t)\cos t - (a + v_0 \cos(\Omega t))\sin t,\\ &-v_0\Omega \sin(\Omega t)\sin t + (b + v_0 \cos(\Omega t))\cos t,\\ &v_0\Omega \cos(\Omega t)).\end{aligned}$$

Under the stated parameter restrictions, the parametrization is uniformly regular. Let

$$e_\theta(t) = (-\sin t, \cos t, 0).$$

A direct calculation gives

$$e_\theta(t) \cdot \gamma'(t) = (a + v_0 \cos(\Omega t))\sin^2 t + (b + v_0 \cos(\Omega t))\cos^2 t \geq \min\{a, b\} - |v_0| > 0.$$

Hence,

$$\|\gamma'(t)\| \geq c_0 := \min\{a, b\} - |v_0| > 0, \qquad t \in I. \tag{2.3}$$

The spatial trace is denoted by $\Gamma = \gamma(I) \subset \mathbb{R}^3$. It need not be globally injective: If $\Omega = m_0/n_0 \in \mathbb{Q}$ in lowest terms, then $\gamma(t + 2\pi n_0) = \gamma(t)$. To treat periodicity and self-intersections without making the arc length coordinate multivalued, we use the parametrized carrier

$$C = C_\gamma := \{\iota(t) = (t, \gamma(t)) : t \in I\} \subset I \times \mathbb{R}^3. \tag{2.4}$$

The map $\iota : I \to C$ is a homeomorphism with its inverse given by projection onto the first coordinate, so distinct parameter values remain distinct in C. Let $\pi : C \to \Gamma$ be the spatial projection defined by $\pi(\iota(t)) = \gamma(t)$. If $J \subseteq I$, and $\gamma|_J$ is a topological embedding (in particular, if J is compact, and $\gamma|_J$ is injective), then with $C_J = \iota(J)$, the restriction $\pi_J := \pi|_{C_J} : C_J \to \gamma(J)$ is a homeomorphism. Thus, C_J can be identified with the embedded branch $\gamma(J)$; Section 5 verifies these conditions for the compact numerical segment.

Throughout the paper, the carrier C is equipped with the measure defined in the parameter chart by

$$d\mu_C(\iota(t)) = \|\gamma'(t)\|\, dt. \tag{2.5}$$

This is the spatial arc length line element carried with multiplicity along the parametrization; it is not the Euclidean graph length element of $C \subset I \times \mathbb{R}^3$, which would be $\sqrt{1 + \|\gamma'(t)\|^2}\, dt$. On every subinterval J satisfying the embedding condition above, π_J pushes $\mu_C|_{C_J}$ forward to the ordinary arc length measure on the embedded spatial branch $\gamma(J)$. At a spatial self-intersection, the parameter labels keep the distinct branches separate, and each passage through the intersection is counted with its own arc length multiplicity. Accordingly, $L^2(C)$ means $L^2(C, d\mu_C)$ throughout.

Define the oriented arc length coordinate

$$s(t) = \int_{t_*}^{t} \|\gamma'(u)\|\, du, \qquad X = s(I) \subseteq \mathbb{R}. \tag{2.6}$$

Because $s'(t) = \|\gamma'(t)\| \geq c_0 > 0$, the map $s : I \to X$ is a strictly increasing homeomorphism and has a continuous inverse $t = t(s)$. The arc length-preserving projection on the parametrized carrier and its inverse are therefore

$$p : C \to X, \qquad p(\iota(t)) = s(t) \tag{2.7}$$

and

$$p^{-1} : X \to C, \qquad p^{-1}(s) = \iota(t(s)). \tag{2.8}$$

They are mutually inverse homeomorphisms. If $I = [T_0, T_1]$, and $t_* = T_0$, then $X = [0, \ell_C]$, where $\ell_C = s(T_1)$. If $I = \mathbb{R}$, then (2.3) implies

$$|s(t)| \geq c_0 |t - t_*| \quad \text{in the corresponding direction,}$$

so $s(t) \to \pm\infty$ as $t \to \pm\infty$, and hence,

$$p(C) = X = \mathbb{R}. \tag{2.9}$$

Thus, the global setting used in Sections 3 and 4 is nonempty for the present curve model: It is the parametrized carrier with $I = \mathbb{R}$, not the generally self-intersecting spatial trace viewed as an unlabelled subset of $\mathbb{R}^3$. On subintervals satisfying the embedding condition above, the restricted carrier and spatial branch are canonically identified. A bounded injective branch is used in Section 5 only to test the numerical arc length map; no unrestricted real line multiresolution assertion is inferred from a finite zero extension. Based on the construction of arc length-preserving projections [6,13], the Euler scheme below computes the discrete parameter map s_N and the corresponding sampled carrier projection p_N. The Euler discretization scheme is obtained from the Cauchy formulation below:

$$\begin{cases} \dfrac{dy}{dt} = f(t, y(t)), \\ y(t_0) = y_0. \end{cases}$$

Let the interval $[T_0, T_1]$ be partitioned as

$$T_0 = t_0 < t_1 < \cdots < t_n = T_1,$$

which divides the interval into n subintervals with step sizes Δt_i, where

$$\Delta t_i = t_i - t_{i-1}, \qquad i = 1, 2, \ldots, n.$$

For computational convenience, a uniform step size is adopted, namely

$$\Delta t_i = \Delta t = \frac{T_1 - T_0}{n}.$$

A key step is to approximate the derivative by using a finite difference quotient. When the step size Δt is sufficiently small, the following approximation holds:

$$\left.\frac{dy}{dt}\right|_{t=t_i} \approx \frac{y(t_i + \Delta t) - y(t_i)}{\Delta t}.$$

The iterative formula of the explicit Euler method is obtained as follows:

$$y(t_{i+1}) \approx y(t_i) + f(t_i, y(t_i))\Delta t.$$

According to Taylor's formula, the Euler discretization scheme is a first-order method. By direct calculation, we obtain

$$\begin{aligned} dL = \Big[&(v_0\Omega)^2 + (a + v_0 \cos(\Omega t))^2 \sin^2 t \\ &+ (b + v_0 \cos(\Omega t))^2 \cos^2 t + 2v_0\Omega(a - b)\sin(\Omega t)\sin t \cos t\Big]^{1/2} dt. \end{aligned} \tag{2.10}$$

Under this scheme, the bounded time domain $[T_0, T_1]$ is partitioned as

$$T_0 = t_0 < t_1 < \cdots < t_n = T_1.$$

For the subinterval $[t_{i-1}, t_i]$, the left-endpoint Euler approximation of the arc length increment is

$$\begin{aligned} \Delta L_i^{(E)} &:= L_i - L_{i-1} = \|\gamma'(t_{i-1})\|\, \Delta t_i \\ &= \Big[(v_0\Omega)^2 + (a + v_0 \cos(\Omega t_{i-1}))^2 \sin^2 t_{i-1} \\ &\qquad + (b + v_0 \cos(\Omega t_{i-1}))^2 \cos^2 t_{i-1} \\ &\qquad + 2v_0\Omega(a - b)\sin(\Omega t_{i-1})\sin t_{i-1} \cos t_{i-1}\Big]^{1/2} \Delta t_i, \qquad \Delta t_i = t_i - t_{i-1}. \end{aligned} \tag{2.11}$$

This is a first-order approximation to the exact increment $\int_{t_{i-1}}^{t_i} \|\gamma'(u)\|\, du$ rather than an exact equivalence with the differential identity. To distinguish the discrete parameter map from the continuous curve projection $p : C \to X$, define the discrete parameter-to-arc length map s_N by

$$\begin{aligned} s_N : \quad t_i \mapsto L_i = L_{i-1} + \Big[&(v_0\Omega)^2 + (a + v_0 \cos(\Omega t_{i-1}))^2 \sin^2 t_{i-1} \\ &+ (b + v_0 \cos(\Omega t_{i-1}))^2 \cos^2 t_{i-1} \\ &+ 2v_0\Omega(a - b)\sin(\Omega t_{i-1})\sin t_{i-1} \cos t_{i-1}\Big]^{1/2} (t_i - t_{i-1})\,. \end{aligned} \tag{2.12}$$

Here, $s_N(t_0) = L_0 = 0$, corresponding to the initial spatial point $(x_0, y_0, z_0) = \gamma(t_0)$. At the grid values L_i, let $t_N = s_N^{-1}$ denote the discrete inverse parameter map, which approximates the continuous inverse parameter function $t = t(s)$ in Eq (2.8):

$$\begin{aligned} t_N : \ L_i \mapsto t_i = t_{i-1} + \Big[& (v_0\Omega)^2 + (a + v_0\cos(\Omega t_{i-1}))^2 \sin^2 t_{i-1} \\ & + (b + v_0\cos(\Omega t_{i-1}))^2 \cos^2 t_{i-1} \\ & + 2v_0\Omega(a-b)\sin(\Omega t_{i-1})\sin t_{i-1}\cos t_{i-1} \Big]^{-1/2} (L_i - L_{i-1}) . \end{aligned} \tag{2.13}$$

$$\gamma(t_i) = ((a + v_0\cos(\Omega t_i))\cos(t_i), (b + v_0\cos(\Omega t_i))\sin(t_i), v_0\sin(\Omega t_i)) . \tag{2.14}$$

Here, L_0 corresponds to t_0, from which the point $(x(t_0), y(t_0), z(t_0))$ is determined.

Accordingly, on the sampled carrier points, the discrete projection and its inverse are

$$p_N(\iota(t_i)) = L_i, \qquad p_N^{-1}(L_i) = \iota(t_N(L_i)) = \iota(t_i). \tag{2.15}$$

The corresponding sampled spatial point is $\pi(p_N^{-1}(L_i)) = \gamma(t_i)$. Thus, s_N and t_N act on the parameter and arc length grids, whereas p_N and p_N^{-1} act between sampled carrier points and sampled arc length coordinates, consistently with the continuous maps in Eqs (2.7) and (2.8).

The Hilbert space identification used in the remainder of the paper is a change-of-variables consequence of the arc length coordinate and follows the length coordinate constructions in [6,13,14]. It is recalled here in notation adapted to the present model, and no novelty is claimed for this isometry. For $\widetilde{f} \in L^2(C)$, define

$$(U\widetilde{f})(s) = \widetilde{f}(\iota(t(s))), \qquad s \in X.$$

Because $ds = \|\gamma'(t)\|dt = d\mu_C$ in the parameter chart,

$$\int_C |\widetilde{f}(\xi)|^2 d\mu_C(\xi) = \int_I |\widetilde{f}(\iota(t))|^2 \|\gamma'(t)\| dt = \int_X |(U\widetilde{f})(s)|^2 ds.$$

Hence, $U : L^2(C, d\mu_C) \to L^2(X)$ is unitary; as stated above, we abbreviate $L^2(C, d\mu_C)$ to $L^2(C)$. Moreover, $(U^{-1}F)(\xi) = F(p(\xi))$. Polarization gives for $\widetilde{f}, \widetilde{g} \in L^2(C)$,

$$\langle \widetilde{f}, \widetilde{g} \rangle_{L^2(C)} = \langle U\widetilde{f}, U\widetilde{g} \rangle_{L^2(X)}, \tag{2.16}$$

and equivalently for $F, G \in L^2(X)$,

$$\langle F, G \rangle_{L^2(X)} = \langle U^{-1}F, U^{-1}G \rangle_{L^2(C)}. \tag{2.17}$$

Only when $X = \mathbb{R}$ is this an identification with the full real line space. Throughout the sequel, $t \in I$ denotes the parameter, $\xi = \iota(t) \in C$ a point of the parametrized carrier, $\pi(\xi) = \gamma(t) \in \Gamma$ its spatial location, $s = p(\xi) \in X$ the arc length coordinate, $x \in \mathbb{R}$ a real line spatial variable, Ω the fixed geometric rotation rate parameter, and $\omega \in \mathbb{R}$ the Fourier frequency dual to s.

The following transport observation is an immediate consequence of unitarity; related one-direction formulations appear in [2,10,11,13,14].

Lemma 2.1. *Let J be countable, and let $(F_k)_{k\in J} \subset L^2(X)$. Set $\widetilde{F}_k = U^{-1}F_k = F_k \circ p$. Then, orthonormal basis, Riesz basis, and frame properties are preserved, including the same Riesz or frame bounds. In the global case $X = \mathbb{R}$, this transports the corresponding real line family to $L^2(C)$.*

2.2. *Overview of two-direction scaling functions*

Yang and Li [15] studied two-direction multiresolution analysis, introduced orthogonal scaling functions and wavelet systems in the two-direction setting, developed related construction procedures, and examined approximation order and regularity. Before presenting the main construction, the basic concept underlying a two-direction multiresolution structure is recalled.

Definition 2.2. Consider a family $(V_j)_{j\in\mathbb{Z}}$ consisting of closed subspaces in $L^2(\mathbb{R})$. The closed subspace V_j is defined by

$$V_j = \mathrm{clos}_{L^2(\mathbb{R})}\left\langle 2^{\frac{j}{2}}\phi(2^jx-k), 2^{\frac{j}{2}}\phi(l-2^jx) : k,l\in\mathbb{Z}\right\rangle. \tag{2.18}$$

We say that $\phi(x)$ generates the multiresolution structure $(V_j)_{j\in\mathbb{Z}}$ in $L^2(\mathbb{R})$ if the closed subspaces defined by Equation (2.18) satisfy the following conditions:

(i) $\cdots \subset V_{-1} \subset V_0 \subset V_1 \subset \cdots$;
(ii) $\mathrm{clos}_{L^2(\mathbb{R})}\left(\bigcup_{j\in\mathbb{Z}} V_j\right) = L^2(\mathbb{R})$;
(iii) $\bigcap_{j\in\mathbb{Z}} V_j = \{0\}$;
(iv) $f(x)\in V_j \Leftrightarrow f(2x)\in V_{j+1}$;
(v) A suitable ϕ can be selected so that

$$\{\phi(x-k), \phi(l-x) : k,l\in\mathbb{Z}\}$$

forms a Riesz basis for V_0.

When this Riesz basis is orthonormal, $(V_j)_{j\in\mathbb{Z}}$ is called an orthogonal two-direction multiresolution analysis, and ϕ is called an orthogonal two-direction scaling function.

The following wavelet discussion concerns this orthogonal special case. At level $j\in\mathbb{Z}$, W_j is specified by

$$V_{j+1} = V_j \oplus W_j.$$

This component corresponds to wavelet level j. When a suitable ψ can be chosen so that

$$\left\{2^{\frac{j}{2}}\psi(2^jx-k), 2^{\frac{j}{2}}\psi(l-2^jx) : k,l\in\mathbb{Z}\right\}$$

constitutes a complete orthogonal system spanning W_j for each $j\in\mathbb{Z}$, then

$$\left\{2^{\frac{j}{2}}\psi(2^jx-k), 2^{\frac{j}{2}}\psi(l-2^jx) : k,l\in\mathbb{Z},\ j\in\mathbb{Z}\right\}$$

also constitutes a complete orthogonal system spanning

$$\overline{\bigoplus_{j\in\mathbb{Z}} W_j} = L^2(\mathbb{R}).$$

Accordingly, ϕ serves as the two-direction scaling function, and ψ serves as the associated wavelet function.

Let $\phi(x)$ be an orthogonal scaling function in the two-direction setting with dilation factor 2, and let ψ denote the wavelet associated with ϕ. The following orthogonality conditions hold:

$$\begin{cases}\langle\phi(x),\phi(x-k)\rangle=\delta_{0,k},\langle\phi(x),\phi(k-x)\rangle=0\\ \langle\phi(x),\psi(x-k)\rangle=0,\langle\phi(x),\psi(k-x)\rangle=0\\ \langle\psi(x),\psi(x-k)\rangle=\delta_{0,k},\langle\psi(x),\psi(k-x)\rangle=0.\end{cases}$$

For dilation factor 2, the two-direction scaling generator and its associated wavelet obey the two-scale refinement relations below:

$$\begin{cases}\phi(x)=\sum\limits_k p_k^+\phi(2x-k)+\sum\limits_l p_l^-\phi(l-2x),\\ \psi(x)=\sum\limits_k q_k^+\phi(2x-k)+\sum\limits_l q_l^-\phi(l-2x).\end{cases}\tag{2.19}$$

Throughout the Fourier-domain calculations in this paper, every mask that occurs in a two-scale symbol is assumed to belong to $\ell^1(\mathbb{Z})$; all explicit masks in Sections 4 and 5 are finitely supported. Consequently, every symbol series converges absolutely and uniformly on $\mathbb{R}$ and defines a continuous 2π-periodic function. The corresponding refinement series converge absolutely in L^2, so the L^2 Fourier transform can be passed through the mask sums by continuity. Applying the Fourier transform to Eq (2.19) gives

$$\begin{cases}\hat{\phi}(\omega)=P^+\left(\frac{\omega}{2}\right)\hat{\phi}\left(\frac{\omega}{2}\right)+P^-\left(\frac{\omega}{2}\right)\hat{\phi}\left(-\frac{\omega}{2}\right),\\ \hat{\psi}(\omega)=Q^+\left(\frac{\omega}{2}\right)\hat{\phi}\left(\frac{\omega}{2}\right)+Q^-\left(\frac{\omega}{2}\right)\hat{\phi}\left(-\frac{\omega}{2}\right).\end{cases}\tag{2.20}$$

Define the symbols as follows:

$$P^+\left(\frac{\omega}{2}\right)=\frac{1}{2}\sum_{k\in\mathbb{Z}}p_k^+e^{-\frac{i\omega k}{2}},\qquad P^-\left(\frac{\omega}{2}\right)=\frac{1}{2}\sum_{k\in\mathbb{Z}}p_k^-e^{-\frac{i\omega k}{2}}.$$

Here, $P^+(\omega/2)$ and $P^-(\omega/2)$ denote the positive- and negative-direction two-scale symbols of ϕ, respectively, and

$$Q^+\left(\frac{\omega}{2}\right)=\frac{1}{2}\sum_{k\in\mathbb{Z}}q_k^+e^{-\frac{i\omega k}{2}},\qquad Q^-\left(\frac{\omega}{2}\right)=\frac{1}{2}\sum_{k\in\mathbb{Z}}q_k^-e^{-\frac{i\omega k}{2}}.$$

Here, $Q^+(\omega/2)$ and $Q^-(\omega/2)$ represent the positive- and negative-direction two-scale symbols of ψ. In the notation above, the complex-valued orthogonality criteria in [15] are most clearly written in Hermitian matrix form. Define

$$\mathcal{P}(\omega)=\begin{bmatrix}P^+(\omega) & P^-(\omega)\\ P^-(-\omega) & P^+(-\omega)\end{bmatrix},$$

$$\mathcal{Q}(\omega)=\begin{bmatrix}Q^+(\omega) & Q^-(\omega)\\ Q^-(-\omega) & Q^+(-\omega)\end{bmatrix}.$$

Assume that the corresponding two-direction refinement equations admit L^2-stable generators and that their integer-translate/reflected families are stable in the associated scale spaces. If $\phi(x)$ is an orthogonal two-direction scaling function, and $\psi(x)$ is its associated orthogonal two-direction wavelet, then for almost every $\omega \in \mathbb{R}$,

$$\begin{cases} \mathcal{P}(\omega)\mathcal{P}(\omega)^* + \mathcal{P}(\omega+\pi)\mathcal{P}(\omega+\pi)^* = I_2, \\ \mathcal{P}(\omega)\mathcal{Q}(\omega)^* + \mathcal{P}(\omega+\pi)\mathcal{Q}(\omega+\pi)^* = 0_{2\times 2}, \\ \mathcal{Q}(\omega)\mathcal{Q}(\omega)^* + \mathcal{Q}(\omega+\pi)\mathcal{Q}(\omega+\pi)^* = I_2. \end{cases} \tag{2.21}$$

Here, * denotes conjugate transpose. The negative-frequency entries are the same ones that arise from the Fourier recursions for $\widehat{\phi}(\omega)$, $\widehat{\phi}(-\omega)$, $\widehat{\psi}(\omega)$, and $\widehat{\psi}(-\omega)$. Thus, Eq (2.21) is a necessary Hermitian mask condition. Its converse is not inferred from L^2 stability and the Riesz property alone; a sufficient conclusion requires additional independently verified hypotheses, such as uniqueness of the normalized Hermitian Gramian fixed point in an applicable matrix mask theorem.

3. Two-direction scaling functions on generalized elliptic helical curves

Throughout Sections 3 and 4, $C = C_\gamma$ denotes the global parametrized carrier with $I = \mathbb{R}$. By (2.3)–(2.9), $p : C \to \mathbb{R}$ is an arc length-preserving homeomorphism. Hence, the unitary map U transports the complete real line two-direction multiresolution structure to $L^2(C)$ without boundary truncation. According to Eqs (2.16) and (2.17), a two-direction multiresolution analysis on $L^2(C)$ can be defined as follows.

Definition 3.1. Suppose that the subspace family $(\nu_j)_{j\in\mathbb{Z}}$ has the properties listed below:

1. The subspaces are nested; namely, each ν_j is contained in the next one for every $j \in \mathbb{Z}$;
2. The intersection of all subspaces in the family is trivial, and their union is dense in $L^2(C)$;
3. For every $j \in \mathbb{Z}$, the scale relation is

   $$f^C \in \nu_j \quad \Longleftrightarrow \quad D_2 f^C \in \nu_{j+1},$$

   where the unitary dyadic dilation is explicitly defined by

   $$(D_2 f^C)(\xi) = 2^{1/2}(f^C \circ p^{-1})(2p(\xi)), \qquad \xi \in C.$$

4. For a suitable real line scaling generator ϕ, set $\phi^C = U^{-1}\phi = \phi \circ p$. Then, the family

   $$\{\phi^{C,+}_{0,k}, \phi^{C,-}_{0,l} : k, l \in \mathbb{Z}\}$$

   constitutes a Riesz basis for ν_0, and the induced subspaces $\{\nu_j\}$ generate a two-direction multiresolution structure in $L^2(C)$, where

   $$\phi^{C,+}_{j,k} = 2^{\frac{j}{2}}\phi(2^j p(\xi) - k),$$

   $$\phi^{C,-}_{j,l} = 2^{\frac{j}{2}}\phi(l - 2^j p(\xi)), \qquad \xi \in C,$$

   $$\nu_j = \mathrm{clos}_{L^2(C)}\left\langle \phi^{C,+}_{j,k}, \phi^{C,-}_{j,l} : k, l \in \mathbb{Z}\right\rangle.$$

When the Riesz basis at scale zero is orthonormal, the structure is called an orthogonal two-direction multiresolution analysis on C.

For every integer index j, define w_j as the subspace that completes v_j to an orthogonal decomposition of v_{j+1}. Equivalently, v_{j+1} admits an orthogonal decomposition into v_j and w_j; hence, any vector in v_{j+1} has unique components in these two subspaces. The component w_j is regarded as the wavelet-level subspace associated with the generalized elliptic helical curve. In the orthogonal special case, when an admissible wavelet ψ is chosen, its curve-induced counterpart $\psi^C = \psi \circ p$ is required to satisfy the following condition: At each integer scale, the collection $\left\{\psi^{C,+}_{j,k}, \psi^{C,-}_{j,l} : k, l \in \mathbb{Z}\right\}$ forms a complete orthogonal basis of w_j. Consequently, the wavelet family

$$\left\{\psi^{C,+}_{j,k}, \psi^{C,-}_{j,l} : j, k, l \in \mathbb{Z}\right\}$$

constitutes a complete orthogonal system in

$$\overline{\bigoplus_{j\in\mathbb{Z}} w_j} = L^2(C).$$

Thus, ϕ^C serves as the two-direction scaling function associated with the generalized elliptic helical curve, whereas ψ^C serves as its corresponding two-direction wavelet. Under the standing hypothesis $X = \mathbb{R}$, let $f^C \in L^2(C)$, and set $F_f = f^C \circ p^{-1} \in L^2(\mathbb{R})$. The curve operators are the unitary pull-backs of the classical real line operators.

(1) Translation operator:
$$(T_b f^C)(\xi) = F_f(p(\xi) - b), \quad b \in \mathbb{R}.$$

(2) Reflected translation operator:
$$(R_b f^C)(\xi) = F_f(b - p(\xi)), \quad b \in \mathbb{R}.$$

(3) Dilation operator:
$$(D_a f^C)(\xi) = a^{1/2} F_f(a p(\xi)), \quad a > 0.$$

The factor $a^{1/2}$ makes D_a unitary on $L^2(C)$; the operators T_b and R_b are also unitary when $X = \mathbb{R}$. If X is a proper interval, define $X^T_b = \{s \in X : s - b \in X\}$, $X^R_b = \{s \in X : b - s \in X\}$ and $X^D_a = \{s \in X : as \in X\}$. The same formulas then define only local operators on $p^{-1}(X^T_b)$, $p^{-1}(X^R_b)$ and $p^{-1}(X^D_a)$, respectively. A zero extension may be used for numerical evaluation, but it is not used to claim a complete global multiresolution analysis (MRA) on a finite segment. Based on the two-direction multiresolution analysis and Eq (2.19), ϕ^C obeys the refinement relation below in the two-direction setting:

$$\phi^C(\xi) = \sum_{k\in\mathbb{Z}} p^{C,+}_k \left(\phi^C \circ p^{-1}\right)(2 \cdot p(\xi) - k) + \sum_{l\in\mathbb{Z}} p^{C,-}_l \left(\phi^C \circ p^{-1}\right)(l - 2 \cdot p(\xi)), \tag{3.1}$$

where $\{p^{C,+}_k\}$ and $\{p^{C,-}_l\}$ are the positive- and negative-direction two-scale coefficient sequences of the curve-based scaling generator ϕ^C on the generalized elliptic helical curve. The associated curve wavelet ψ^C satisfies the refinement relation below in the two-direction setting:

$$\psi^C(\xi) = \sum_{k\in\mathbb{Z}} q^{C,+}_k \left(\phi^C \circ p^{-1}\right)(2 \cdot p(\xi) - k) + \sum_{l\in\mathbb{Z}} q^{C,-}_l \left(\phi^C \circ p^{-1}\right)(l - 2 \cdot p(\xi)), \tag{3.2}$$

where $\{q_k^{C,+}\}$ and $\{q_l^{C,-}\}$ denote the positive- and negative-direction refinement sequences associated with the two-direction wavelet ψ^C on the generalized elliptic helical curve. Let $\phi = \phi^C \circ p^{-1}$ be the real line function obtained through the arc length-preserving map p. The function ϕ is assumed to obey Eq (2.19):

$$\phi(x) = \sum_k p_k^+ \phi(2x-k) + \sum_l p_l^- \phi(l-2x).$$

Here, $\{p_k^+\}$ and $\{p_l^-\}$ are the positive- and negative-direction two-scale coefficient sequences of the two-direction scaling generator ϕ, respectively. Their relationship with $\{p_k^{C,+}\}$ and $\{p_l^{C,-}\}$ is stated below.

Lemma 3.1. *Let $p : C \to \mathbb{R}$ be the global arc length-preserving projection, where $C = C_\gamma$ denotes the global parametrized carrier of the generalized elliptic helical curve. Suppose that, through p, a curve-based two-direction scaling generator $\phi^C \in L^2(C)$ is obtained from a function $\phi \in L^2(\mathbb{R})$ as*

$$\phi^C = \phi \circ p.$$

Assume that ϕ obeys the refinement Eq (2.19), whereas ϕ^C obeys the curve-based refinement Eq (3.1). Assume further that the scale-one two-direction scaling family

$$\{\phi_{1,k}^{C,+}, \phi_{1,l}^{C,-} : k, l \in \mathbb{Z}\}$$

is a Riesz basis (orthogonal in the orthogonal case) of the scale space v_1. Assume in addition that the real line and curve coefficient pairs belong to $\ell^2(\mathbb{Z}) \times \ell^2(\mathbb{Z})$ and that both refinement expansions are interpreted as unconditionally convergent series in the L^2 norm. Then, the corresponding refinement coefficients coincide, namely,

$$p_k^{C,+} = p_k^+, \qquad p_l^{C,-} = p_l^-.$$

Proof. Because the projection p preserves arc length, it induces an isometric correspondence between functions on the real line and functions on the curve C. In particular, we have

$$\phi^C = \phi \circ p \qquad \text{or equivalently,} \qquad \phi = \phi^C \circ p^{-1}.$$

Starting from the refinement equation of ϕ on $\mathbb{R}$,

$$\phi(x) = \sum_k p_k^+ \phi(2x-k) + \sum_l p_l^- \phi(l-2x),$$

and substituting $x = p(\xi)$, we obtain

$$\phi(p(\xi)) = \sum_k p_k^+ \phi(2p(\xi)-k) + \sum_l p_l^- \phi(l-2p(\xi)).$$

Using $\phi^C(\xi) = \phi(p(\xi))$ and $\phi = \phi^C \circ p^{-1}$, this becomes

$$\phi^C(\xi) = \sum_k p_k^+ \left(\phi^C \circ p^{-1}\right)(2p(\xi)-k) + \sum_l p_l^- \left(\phi^C \circ p^{-1}\right)(l-2p(\xi)).$$

On the other hand, by Eq (3.1),

$$\phi^C(\xi) = \sum_k p_k^{C,+} \left(\phi^C \circ p^{-1}\right)(2p(\xi)-k) + \sum_l p_l^{C,-} \left(\phi^C \circ p^{-1}\right)(l-2p(\xi)).$$

By the stated ℓ^2 assumptions and unconditional L^2 convergence, both displayed expressions are legitimate expansions of the same element $\phi^C \in \nu_1$ in the scale-one two-direction scaling family. The un-normalized functions in the refinement equations differ from $\phi^{C,+}_{1,k}$ and $\phi^{C,-}_{1,l}$ only by the common nonzero factor $2^{-1/2}$, so they also form a Riesz basis of ν_1. The uniqueness of the ℓ^2 Riesz basis expansion therefore permits coefficient comparison. Hence, comparison of the two refinement equations yields

$$p^{C,+}_k = p^+_k, \qquad p^{C,-}_l = p^-_l.$$

The proof is therefore complete. □

Lemma 3.2. *Let $p : C \to \mathbb{R}$ be the global arc length-preserving projection, where $C = C_\gamma$ denotes the global parametrized carrier of the generalized elliptic helical curve. Suppose that, through p, ϕ^C on C is obtained from an orthogonal two-direction scaling generator $\phi \in L^2(\mathbb{R})$, and ψ^C is obtained from the associated orthogonal two-direction wavelet generator $\psi \in L^2(\mathbb{R})$. Assume that the scale-one two-direction scaling family*

$$\{\phi^{C,+}_{1,k}, \phi^{C,-}_{1,l} : k, l \in \mathbb{Z}\}$$

is a Riesz basis (orthogonal in the orthogonal case) of the scale space ν_1. Assume in addition that the real line and curve wavelet coefficient pairs belong to $\ell^2(\mathbb{Z}) \times \ell^2(\mathbb{Z})$ and that both wavelet refinement expansions converge unconditionally in the L^2 norm. Then, the wavelet refinement coefficients are invariant under this projection:

$$q^{C,+}_k = q^+_k, \qquad q^{C,-}_l = q^-_l.$$

Proof. Here, $\{q^+_k\}$ and $\{q^-_l\}$ are the coefficient sequences in Eq (2.19), whereas $\{q^{C,+}_k\}$ and $\{q^{C,-}_l\}$ are the corresponding coefficient sequences in Eq (3.2). The argument follows the same idea as Lemma 3.1. Starting from the real line wavelet refinement equation and substituting $x = p(\xi)$, the induced curve wavelet satisfies

$$\psi^C(\xi) = \sum_k q^+_k \left(\phi^C \circ p^{-1}\right)(2p(\xi) - k) + \sum_l q^-_l \left(\phi^C \circ p^{-1}\right)(l - 2p(\xi)).$$

By the stated ℓ^2 assumptions and unconditional L^2 convergence, both this expression and Eq (3.2) are legitimate expansions of the same element $\psi^C \in \nu_1$ in the scale-one two-direction scaling family. The un-normalized functions appearing in the two refinement equations differ from $\phi^{C,+}_{1,k}$ and $\phi^{C,-}_{1,l}$ only by the common nonzero factor $2^{-1/2}$; hence, they also form a Riesz basis of ν_1. The uniqueness of the ℓ^2 Riesz basis expansion therefore permits coefficient comparison. Thus, comparing this expression with Eq (3.2) yields

$$q^{C,+}_k = q^+_k, \qquad q^{C,-}_l = q^-_l.$$

□

Under the standing hypothesis $X = \mathbb{R}$, a curve function $f^C \in L^2(C)$ is represented by $F_f(s) = f^C(p^{-1}(s)) \in L^2(\mathbb{R})$. If $F_f \in L^1(\mathbb{R}) \cap L^2(\mathbb{R})$, its Fourier transform on the curve is defined through the arc length coordinate by

$$\widehat{f^C}(\omega) = \widehat{F_f}(\omega) = \int_{\mathbb{R}} F_f(s) e^{-i\omega s}\, ds, \qquad \omega \in \mathbb{R}. \tag{3.3}$$

For a general $F_f \in L^2(\mathbb{R})$, $\widehat{f^C}$ is defined by the unique Plancherel extension of this transform; consequently, the Fourier identities below are understood in the L^2 sense and hence, almost everywhere. Here, $\xi \in C$ is a point of the parametrized carrier, $s = p(\xi)$ is its arc length coordinate, and ω is the real frequency variable. Thus, no carrier point or spatial point is used as a spectral variable. Under the standing ℓ^1-mask assumption, the curve refinement series converges absolutely in $L^2(C)$, and its Fourier transform may be evaluated term by term in the L^2 sense. Applying this definition to Eq (3.1) and writing $F(\omega) = \widehat{\phi^C \circ p^{-1}}(\omega)$ gives

$$F(\omega) = P^{C,+}\left(\frac{\omega}{2}\right)F\left(\frac{\omega}{2}\right) + P^{C,-}\left(\frac{\omega}{2}\right)F\left(-\frac{\omega}{2}\right), \tag{3.4}$$

where

$$P^{C,+}\left(\frac{\omega}{2}\right) = \frac{1}{2}\sum_{k\in\mathbb{Z}} p_k^{C,+}e^{-ik\omega/2}, \qquad P^{C,-}\left(\frac{\omega}{2}\right) = \frac{1}{2}\sum_{k\in\mathbb{Z}} p_k^{C,-}e^{-ik\omega/2}. \tag{3.5}$$

Replacing ω by $-\omega$ gives

$$F(-\omega) = P^{C,+}\left(-\frac{\omega}{2}\right)F\left(-\frac{\omega}{2}\right) + P^{C,-}\left(-\frac{\omega}{2}\right)F\left(\frac{\omega}{2}\right). \tag{3.6}$$

By combining relations (3.4) and (3.6), one obtains

$$\begin{bmatrix} F(\omega) \\ F(-\omega) \end{bmatrix} = \begin{bmatrix} P^{C,+}\left(\frac{\omega}{2}\right) & P^{C,-}\left(\frac{\omega}{2}\right) \\ P^{C,-}\left(-\frac{\omega}{2}\right) & P^{C,+}\left(-\frac{\omega}{2}\right) \end{bmatrix} \begin{bmatrix} F\left(\frac{\omega}{2}\right) \\ F\left(-\frac{\omega}{2}\right) \end{bmatrix}. \tag{3.7}$$

Define the Fourier-side vector and mask matrix by

$$\mathbf{F}(\omega) = \begin{bmatrix} F(\omega) \\ F(-\omega) \end{bmatrix}, \qquad \mathcal{M}_C(\eta) = \begin{bmatrix} P^{C,+}(\eta) & P^{C,-}(\eta) \\ P^{C,-}(-\eta) & P^{C,+}(-\eta) \end{bmatrix}. \tag{3.8}$$

Then, Eq (3.7) is $\mathbf{F}(\omega) = \mathcal{M}_C(\omega/2)\mathbf{F}(\omega/2)$. Iterating this identity only a finite number of times gives for every integer $J \geq 1$,

$$\mathbf{F}(\omega) = \left(\prod_{j=1}^{J} \mathcal{M}_C\left(\frac{\omega}{2^j}\right)\right)\mathbf{F}\left(\frac{\omega}{2^J}\right), \tag{3.9}$$

where the ordered product means $\prod_{j=1}^{J} A_j = A_1 A_2 \cdots A_J$. For a normalized refinable solution whose Fourier representative is continuous at the origin with $F(0) = 1$, the terminal vector in (3.9) satisfies

$$\mathbf{F}\left(\frac{\omega}{2^J}\right) \longrightarrow \begin{bmatrix} F(0) \\ F(0) \end{bmatrix} \qquad (J \to \infty).$$

This convergence of the terminal vector alone does not justify replacing the finite product by an infinite product. The matrix limit

$$\mathcal{P}_C(\omega) := \lim_{J\to\infty} \prod_{j=1}^{J} \mathcal{M}_C\left(\frac{\omega}{2^j}\right) \tag{3.10}$$

must be established separately in the mode of convergence required by the cascade theorem. Only when this limit exists and passage to the limit in (3.9) is justified may one conclude that

$$\mathbf{F}(\omega) = \mathcal{P}_C(\omega) \begin{bmatrix} F(0) \\ F(0) \end{bmatrix}.$$

Here, $\omega \in \mathbb{R}$ is the real frequency variable dual to the arc length coordinate $s = p(\xi)$; it is neither a carrier point nor a spatial point. The next statement separates the properties that were previously conflated: The spectral test, existence of a refinable solution, L^2 stability, continuity, and orthogonality.

Theorem 3.1. *Let $p : C \to \mathbb{R}$ be the global arc length coordinate, let U be the unitary map above, and assume that $(p_k^{C,+})_{k\in\mathbb{Z}}, (p_k^{C,-})_{k\in\mathbb{Z}} \in \ell^1(\mathbb{Z})$. Let $\mathcal{M}_C$ be the resulting continuous 2π-periodic mask matrix defined in Eq* (3.8)*. The following assertions are logically distinct.*

1. *The mask matrix spectral condition used in this paper is the statement that $\mathcal{M}_C(0)$ has a simple eigenvalue* 1 *and that all its other eigenvalues have modulus strictly smaller than* 1*. It is distinct from Condition E imposed on the transition operator in the L^2-stability criterion of [15]. In this paper, the zero-frequency condition is treated only as an algebraic property of $\mathcal{M}_C(0)$ and is not used by itself to assert the existence or uniqueness of a compactly supported distributional solution. Any such existence statement must instead be obtained from an applicable refinement equation theorem after all of that theorem's mask, normalization, and compatibility hypotheses have been verified. The zero-frequency condition also does not imply L^2 cascade convergence, L^2 stability, continuity, the Riesz basis property, or orthogonality.*
2. *Suppose, independently, that the associated real line matrix cascade converges in $L^2(\mathbb{R})$ to a refinable function ϕ and that $\{\phi(\cdot - k), \phi(k - \cdot) : k \in \mathbb{Z}\}$ is a Riesz basis for its scale space with bounds A, B. Then, $\phi^C = U^{-1}\phi = \phi \circ p$ satisfies the curve refinement equation, the transported cascade converges in $L^2(C)$, and the corresponding curve family has the same Riesz bounds A, B.*
3. *If the real line solution ϕ is continuous, then $\phi^C = \phi \circ p$ is continuous because $p : C \to \mathbb{R}$ is a homeomorphism. Conversely, continuity may be transported from the curve to the line through the continuous inverse p^{-1}. Neither statement is a consequence of the mask matrix spectral condition alone.*
4. *Orthogonality is not implied by the mask matrix spectral condition or by Riesz stability. An orthogonal generator necessarily satisfies the Hermitian paraunitary mask identity in Theorem 4.1; the reverse implication requires additional sufficiency hypotheses and is not asserted here.*

Thus, the mask matrix spectral condition is used only as a zero-frequency algebraic test. Before the L^2 transport conclusion in item 2 can be invoked, the existence of the relevant real line refinable solution, cascade convergence, L^2 stability, and the Riesz basis property must all be verified separately.

Proof. Item 1 first records the definition of the mask matrix spectral condition for the matrix $\mathcal{M}_C(0)$. It also makes explicit that this zero-frequency algebraic condition is not, by itself, an existence or uniqueness theorem for a compactly supported distributional solution. Such a conclusion requires a separate applicable refinement equation theorem with all of its hypotheses verified. The spectral condition likewise does not provide the additional L^2 conclusions in items 2–4. For item 2, let $(\phi_n)_{n\geq 0}$ denote the real line cascade approximants, and set $\phi_n^C = U^{-1}\phi_n$. Because U is unitary,

$$\|\phi_n^C - \phi^C\|_{L^2(C)} = \|\phi_n - \phi\|_{L^2(\mathbb{R})} \longrightarrow 0.$$

Applying U^{-1} to the real line refinement equation gives the curve refinement equation because $U^{-1}f = f \circ p$, and the refinement coefficients are unchanged under this transport. Moreover, for every finitely supported pair of coefficient sequences (a_k) and (b_k), unitarity gives

$$\left\| \sum_k a_k \phi^{C,+}_{0,k} + \sum_k b_k \phi^{C,-}_{0,k} \right\|_{L^2(C)} = \left\| \sum_k a_k \phi(\cdot - k) + \sum_k b_k \phi(k - \cdot) \right\|_{L^2(\mathbb{R})}.$$

Therefore, the real line Riesz inequalities transfer verbatim, with the same bounds A and B.

For item 3, the continuity of $\phi^C = \phi \circ p$ follows from the continuity of ϕ and the homeomorphism p. Conversely, $\phi = \phi^C \circ p^{-1}$ is continuous whenever ϕ^C is continuous. Finally, the mask matrix spectral condition concerns only the spectrum of $\mathcal{M}_C(0)$, whereas orthogonality necessarily entails the independent all-frequency Hermitian identity stated in Theorem 4.1. Hence, neither the mask matrix spectral condition, the Riesz inequalities, nor the mask identity by itself is used here to infer orthogonality. □

The coefficient alternatives below characterize only the mask matrix spectral condition as a matrix spectral property. They are not presented as an existence or uniqueness theorem for a compactly supported distributional solution. Moreover, the normalization $F(0) = 1$ selects only the second of the two algebraic alternatives below. Neither alternative by itself establishes the existence of a refinable solution, L^2 cascade convergence, continuity, L^2 Riesz stability, or orthogonality.

Theorem 3.2. *Let $p : C \to \mathbb{R}$ be the global arc length coordinate, and let $\phi^C \in L^2(C)$ satisfy the two-direction refinement relation* (3.1)*. Assume $(p^{C,+}_k)_{k\in\mathbb{Z}}, (p^{C,-}_k)_{k\in\mathbb{Z}} \in \ell^1(\mathbb{Z})$ so that all coefficient sums below converge absolutely. The following alternatives for the coefficient sequences $\{p^{C,+}_k\}$ and $\{p^{C,-}_k\}$ are equivalent to the mask matrix spectral condition for $\mathcal{M}_C(0)$:*

$$\begin{cases} \sum_k \left(p^{C,+}_k - p^{C,-}_k\right) = 2, \\ \left|\sum_k \left(p^{C,+}_k + p^{C,-}_k\right)\right| < 2 \end{cases} \quad \textit{or} \quad \begin{cases} \sum_k \left(p^{C,+}_k + p^{C,-}_k\right) = 2, \\ \left|\sum_k \left(p^{C,+}_k - p^{C,-}_k\right)\right| < 2. \end{cases}$$

If a Fourier representative F of a refinable solution is continuous at the origin and normalized by $F(0) = 1$, then only the second alternative is compatible with the refinement equation; equivalently, the eigenvalue 1 *must correspond to the symmetric vector* $[1, 1]^\mathsf{T}$*. The first alternative is only the other algebraic way in which $\mathcal{M}_C(0)$ can satisfy the mask matrix spectral condition and is incompatible with this normalization.*

Proof. By the definitions of the two-scale symbols at the origin, we have

$$\begin{bmatrix} P^{C,+}(0) & P^{C,-}(0) \\ P^{C,-}(0) & P^{C,+}(0) \end{bmatrix} = \begin{bmatrix} \frac{1}{2}\sum_{k\in\mathbb{Z}} p^{C,+}_k & \frac{1}{2}\sum_{k\in\mathbb{Z}} p^{C,-}_k \\ \frac{1}{2}\sum_{k\in\mathbb{Z}} p^{C,-}_k & \frac{1}{2}\sum_{k\in\mathbb{Z}} p^{C,+}_k \end{bmatrix}.$$

Therefore, its eigenvalues are $(1/2)\sum_k \left(p^{C,+}_k - p^{C,-}_k\right)$ and $(1/2)\sum_k \left(p^{C,+}_k + p^{C,-}_k\right)$. Using the two explicit eigenvalues, the mask matrix spectral condition is equivalent to

$$\begin{cases} \sum_k \left(p^{C,+}_k - p^{C,-}_k\right) = 2, \\ \left|\sum_k \left(p^{C,+}_k + p^{C,-}_k\right)\right| < 2 \end{cases} \quad \text{or} \quad \begin{cases} \sum_k \left(p^{C,+}_k + p^{C,-}_k\right) = 2, \\ \left|\sum_k \left(p^{C,+}_k - p^{C,-}_k\right)\right| < 2. \end{cases}$$

For the normalization used in the subsequent Fourier analysis, evaluate the refinement recursion at $\omega = 0$. Because $F(0) = 1$, one has

$$\begin{bmatrix}1\\1\end{bmatrix} = \mathbf{F}(0) = \mathcal{M}_C(0)\mathbf{F}(0) = \mathcal{M}_C(0)\begin{bmatrix}1\\1\end{bmatrix}.$$

Consequently,

$$P^{C,+}(0) + P^{C,-}(0) = 1, \qquad \sum_k (p_k^{C,+} + p_k^{C,-}) = 2.$$

Thus, only the second alternative is compatible with $F(0) = 1$; in the first alternative, the eigenvalue 1 is attached to the antisymmetric vector $[1, -1]^{\mathsf{T}}$. □

In Theorem 3.2, the matrix

$$\begin{bmatrix}P^{C,+}(0) & P^{C,-}(0)\\ P^{C,-}(0) & P^{C,+}(0)\end{bmatrix}$$

satisfies the mask matrix spectral condition precisely when one of the two displayed alternatives holds. For a Fourier representative continuous at the origin and normalized by $F(0) = 1$, only the second alternative is admissible. These algebraic alternatives do not establish the existence or uniqueness of a compactly supported distributional solution. If an external existence theorem is invoked, all of its mask, normalization, and compatibility hypotheses must be checked independently. The alternatives also do not establish L^2 cascade convergence, continuity, or L^2 and Riesz stability. Orthogonality must satisfy the necessary Hermitian condition in Theorem 4.1, and any converse conclusion requires additional independently verified sufficiency hypotheses.

4. Orthogonality and high approximation order of two-direction scaling functions on generalized elliptic helical curves

Definition 4.1. Let $p : C \to \mathbb{R}$ be the global arc length-preserving projection, where $C = C_\gamma$ denotes the global parametrized carrier of the generalized elliptic helical curve. Assume that $\phi^C = \phi \circ p$ for some $\phi \in L^2(\mathbb{R})$. Suppose further that the following conditions hold:

$$\begin{aligned} \left\langle \phi^C, T_k\phi^C \right\rangle_{L^2(C)} &= \delta_{0,k}, \\ \left\langle \phi^C, R_k\phi^C \right\rangle_{L^2(C)} &= 0, \qquad k \in \mathbb{Z}. \end{aligned} \tag{4.1}$$

Then, ϕ^C is referred to as an orthogonal scaling function in the two-direction setting on the generalized elliptic helical curve.

Theorem 4.1. *Fix the global arc length-preserving projection $p : C \to \mathbb{R}$, where $C = C_\gamma$ denotes the global parametrized carrier of the generalized elliptic helical curve. Assume the independent existence and Riesz stability hypotheses in item 2 of Theorem 3.1: The corresponding refinement equation admits a normalized L^2-stable solution ϕ^C with $\|\phi^C\|_{L^2(C)} = 1$, whose two-direction integer-translate/reflected family is a Riesz basis of its closed scale space. Assume also that its positive- and negative-direction* *masks belong to $\ell^1(\mathbb{Z})$. Let $P^{C,+}$ and $P^{C,-}$ be the resulting continuous positive- and negative-direction two-scale symbols of ϕ^C, and define*

$$\mathcal{M}_C(\eta) = \begin{bmatrix} P^{C,+}(\eta) & P^{C,-}(\eta) \\ P^{C,-}(-\eta) & P^{C,+}(-\eta) \end{bmatrix}. \tag{4.2}$$

If ϕ^C is orthogonal, then for almost every $\eta \in \mathbb{R}$,

$$\mathcal{M}_C(\eta)\mathcal{M}_C(\eta)^* + \mathcal{M}_C(\eta+\pi)\mathcal{M}_C(\eta+\pi)^* = I_2. \tag{4.3}$$

Here, * denotes the conjugate transpose. Equivalently,

$$\begin{cases} |P^{C,+}(\eta)|^2 + |P^{C,-}(\eta)|^2 + |P^{C,+}(\eta+\pi)|^2 + |P^{C,-}(\eta+\pi)|^2 = 1, \\ P^{C,+}(\eta)\overline{P^{C,-}(-\eta)} + P^{C,-}(\eta)\overline{P^{C,+}(-\eta)} \\ \quad + P^{C,+}(\eta+\pi)\overline{P^{C,-}(-\eta+\pi)} + P^{C,-}(\eta+\pi)\overline{P^{C,+}(-\eta+\pi)} = 0. \end{cases} \tag{4.4}$$

The second diagonal identity in (4.3) follows from the first one after replacing η by $-\eta$. For real mask coefficients, $P^{C,\pm}(-\eta) = \overline{P^{C,\pm}(\eta)}$, and the displayed cross relation reduces to the corresponding real coefficient formula. These relations are necessary under the stated assumptions. No converse is claimed without an additional independently verified matrix mask sufficiency hypothesis, such as the uniqueness of the normalized Hermitian Gramian fixed point.

Proof. The Fourier recursion derived in Section 3 is

$$\widehat{\mathbf{\Phi}}(2\eta) = \mathcal{M}_C(\eta)\widehat{\mathbf{\Phi}}(\eta), \qquad \widehat{\mathbf{\Phi}}(\eta) := \begin{bmatrix} F(\eta) \\ F(-\eta) \end{bmatrix},$$

where $\mathbf{\Phi} = (\phi, \phi(-\,\cdot))^{\mathsf{T}}$ in the real line arc length coordinate. Thus, the lower row necessarily contains the symbols evaluated at $-\eta$. By the arc length isometry, orthogonality on C is equivalent to orthogonality of the integer translates of the two components of $\mathbf{\Phi}$. Hence, the Hermitian Gramian

$$\mathcal{G}(\eta) := \sum_{k\in\mathbb{Z}} \widehat{\mathbf{\Phi}}(\eta + 2\pi k)\widehat{\mathbf{\Phi}}(\eta + 2\pi k)^*$$

satisfies $\mathcal{G}(\eta) = I_2$ for almost every η. Splitting the sum defining $\mathcal{G}(2\eta)$ into even and odd indices and using the 2π-periodicity of $\mathcal{M}_C$ gives the standard vector refinement identity

$$\mathcal{G}(2\eta) = \mathcal{M}_C(\eta)\mathcal{G}(\eta)\mathcal{M}_C(\eta)^* + \mathcal{M}_C(\eta+\pi)\mathcal{G}(\eta+\pi)\mathcal{M}_C(\eta+\pi)^*.$$

Substituting $\mathcal{G} = I_2$ yields (4.3). This is the Hermitian Gramian/perfect reconstruction calculation underlying the orthogonality criterion in Section 5 of [15]. Expanding the $(1,1)$ and $(1,2)$ entries gives (4.4); the remaining entries are their conjugate and reflected counterparts. This proves the necessary implication. The stated existence and Riesz stability assumptions do not, by themselves, establish the reverse implication. □

Next, we record how an independently verified Hermitian mask identity is transported from the real line to the generalized elliptic helical carrier.

Proposition 4.1. *Let P^+ and P^- be two-scale symbols generated by finitely supported masks and form the structured matrix symbol*

$$\mathcal{M}(\eta) = \begin{bmatrix} P^+(\eta) & P^-(\eta) \\ P^-(-\eta) & P^+(-\eta) \end{bmatrix}.$$

Assume that

$$\mathcal{M}(\eta)\mathcal{M}(\eta)^* + \mathcal{M}(\eta+\pi)\mathcal{M}(\eta+\pi)^* = I_2 \quad \text{for a.e. } \eta.$$

Assume separately that the real line refinement equation generated by these masks has a normalized L^2-stable solution ϕ whose two-direction integer-translate/reflected family is a Riesz basis. If $p : C \to \mathbb{R}$ is the global arc length coordinate, and $\phi^C = \phi \circ p$, then the curve symbols satisfy the same Hermitian identity. Hence, the transported mask passes the necessary mask test in Theorem 4.1. This conclusion does not upgrade the Riesz family to an orthonormal one and does not infer orthogonality; a converse requires a separate matrix mask sufficiency theorem with its additional hypotheses, such as the uniqueness of the normalized Hermitian Gramian fixed point. The zero-frequency mask matrix spectral condition may be checked independently, but it is not needed for the transport asserted in this proposition and does not imply L^2 stability, the Riesz basis property, or orthogonality.

Proof. Lemma 3.1 shows that the arc length isometry leaves the positive- and negative-direction coefficient sequences unchanged. Therefore, the real line symbols and the corresponding curve symbols are identical functions of the arc length frequency, and the displayed Hermitian identity transfers verbatim. The final statements merely delimit this necessary algebraic test from the separate existence, stability, and orthogonality questions. □

For $\sigma \geq 0$, let $H^\sigma(\mathbb{R})$ denote the Bessel-potential Sobolev space

$$H^\sigma(\mathbb{R}) = \left\{ f \in L^2(\mathbb{R}) : \int_{\mathbb{R}} (1 + |\omega|^2)^\sigma |\widehat{f}(\omega)|^2 \, d\omega < \infty \right\}.$$

In the approximation discussion below, saying that the Sobolev regularity index is at least $r > 0$ means membership in $H^\sigma(\mathbb{R})$ for every real $0 \leq \sigma < r$; no membership at the critical endpoint $H^r(\mathbb{R})$ is asserted.

Lemma 4.1. *Let $M, L \in \mathbb{N}$ be positive integers. Let $\phi \in L^2(\mathbb{R})$ be a compactly supported two-direction refinable generator with dilation factor 2. Assume that its two-direction translates and reflected translates form a Riesz basis of V_0, that the associated spaces $(V_j)_{j\in\mathbb{Z}}$ form the real line multiresolution structure used here, and that its finitely supported masks satisfy Eq (2.19). Define the positive- and negative-direction symbols by*

$$P^+(\omega) = \frac{1}{2} \sum_{k\in\mathbb{Z}} p_k^+ e^{-ik\omega} = \left(\frac{1 + e^{-i\omega}}{2} \right)^M S^+(\omega),$$

$$P^-(\omega) = \frac{1}{2} \sum_{k\in\mathbb{Z}} p_k^- e^{-ik\omega} = \left(\frac{1 + e^{-i\omega}}{2} \right)^L S^-(\omega).$$

Here,

$$S^+(\omega) = \sum_{k\in\mathbb{Z}} s_k^+ e^{-ik\omega}, \qquad S^-(\omega) = \sum_{k\in\mathbb{Z}} s_k^- e^{-ik\omega}, \qquad s_k^+ \geq 0, \quad s_k^- \geq 0.$$

If, in addition,

$$\begin{cases} S^+(0) + S^-(0) = 1, & \\ S^-(\pi) \neq 0, & M > L, \\ S^+(\pi) \neq 0, & L > M, \\ S^+(\pi) + e^{-i\pi L} S^-(\pi) \neq 0, & L = M, \end{cases}$$

then ϕ has approximation order $n = \min(L, M)$ in the polynomial reproduction sense of Definition 3 in [15]; namely, every polynomial of degree at most $n-1$ can be represented by a linear combination of the integer translates of $\phi(x)$ and $\phi(-x)$. Moreover,

$$\phi \in H^\sigma(\mathbb{R}) \qquad \textit{for every real } 0 \leq \sigma < n - \frac{1}{2}.$$

No membership at the critical endpoint $H^{n-1/2}(\mathbb{R})$ is claimed.

Proof. Theorem 11 in [15], specialized to the dilation factor $m = 2$ and interpreted through Definition 3 of that paper, gives a polynomial reproduction approximation order $n = \min(L, M)$ and regularity at least $n - 1/2$. For the regularity statement used below, this yields the nonendpoint consequence

$$\phi \in H^\sigma(\mathbb{R}) \qquad \text{for every real } 0 \leq \sigma < n - \frac{1}{2},$$

and no membership at the critical endpoint is asserted. □

The approximation order in Lemma 4.1 is the polynomial reproduction notion used in [15]. It is not identified here without an additional theorem, with a Sobolev best approximation estimate. To obtain the latter, the required real line Jackson estimate is imposed explicitly in the following transport theorem; in an application, it may be verified by an appropriate Strang–Fix theorem after all stability, polynomial reproduction, and nondegeneracy assumptions of that theorem have been checked.

Theorem 4.2. *Let $p : C \to \mathbb{R}$ be the global arc length coordinate, and let $U : L^2(C) \to L^2(\mathbb{R})$ be the associated unitary map. For every real $\sigma \geq 0$, define the arc length Bessel potential Sobolev space*

$$H^\sigma_p(C) := U^{-1} H^\sigma(\mathbb{R}), \qquad \|f^C\|_{H^\sigma_p(C)} := \|U f^C\|_{H^\sigma(\mathbb{R})}.$$

For an integer $n \geq 1$, write $W^n_{2,p}(C) := H^n_p(C)$ and $W^n_2(\mathbb{R}) := H^n(\mathbb{R})$. For each $j \in \mathbb{Z}$, set

$$V^C_j = U^{-1}(V_j) = \{G \circ p : G \in V_j\},$$

and define the real line and curve best approximation errors by

$$E_j(F) := \inf_{G \in V_j} \|F - G\|_{L^2(\mathbb{R})}, \qquad E^C_j(f^C) := \inf_{g^C \in V^C_j} \|f^C - g^C\|_{L^2(C)}.$$

The curve spaces are said to have Sobolev best approximation order n in arc length if there is a constant K independent of f^C and j such that

$$E^C_j(f^C) \leq K 2^{-jn} \|f^C\|_{W^n_{2,p}(C)}$$

for every $f^C \in W^n_{2,p}(C)$ and all sufficiently large j.

Assume that the real line generator ϕ satisfies every stability, multiresolution, factorization, and nonvanishing hypothesis of Lemma 4.1, and put $n = \min(L, M)$ and $\phi^C = \phi \circ p$. Assume, independently, that the associated real line spaces satisfy the Jackson-type estimate

$$E_j(F) \leq K2^{-jn}\|F\|_{W^n_2(\mathbb{R})} \tag{4.5}$$

for every $F \in W^n_2(\mathbb{R})$ and all sufficiently large j, with a constant K independent of F and j. Then, for every $f^C \in L^2(C)$,

$$E^C_j(f^C) = E_j(Uf^C).$$

Consequently, for every $f^C \in W^n_{2,p}(C)$ and all sufficiently large j,

$$E^C_j(f^C) \leq K2^{-jn}\|f^C\|_{W^n_{2,p}(C)}. \tag{4.6}$$

Thus, V^C_j has the same Sobolev best approximation order n as V_j, with the same constant K. Moreover, the regularity conclusion of Lemma 4.1 is transported independently by unitarity:

$$\phi^C \in H^\sigma_p(C) \qquad \text{for every real } 0 \leq \sigma < n - \frac{1}{2},$$

and no membership at the critical endpoint $H^{n-1/2}_p(C)$ is asserted.

Proof. For every $G \in V_j$, set $g^C = U^{-1}G \in V^C_j$. Conversely, every element of V^C_j has this form. By unitarity,

$$\|f^C - g^C\|_{L^2(C)} = \|Uf^C - G\|_{L^2(\mathbb{R})}.$$

Taking the infimum over $G \in V_j$ gives

$$E^C_j(f^C) = E_j(Uf^C).$$

If $f^C \in W^n_{2,p}(C)$, then $Uf^C \in W^n_2(\mathbb{R})$, and by the definition of the transported Sobolev norm,

$$\|Uf^C\|_{W^n_2(\mathbb{R})} = \|f^C\|_{W^n_{2,p}(C)}.$$

Applying the independently assumed real line estimate (4.5) to $F = Uf^C$ therefore yields

$$E^C_j(f^C) = E_j(Uf^C) \leq K2^{-jn}\|Uf^C\|_{W^n_2(\mathbb{R})} = K2^{-jn}\|f^C\|_{W^n_{2,p}(C)},$$

which proves (4.6). This argument transports an already established real line best approximation estimate; it does not derive that estimate from the mask factorization alone. Finally, because $\phi^C = U^{-1}\phi$, the Sobolev regularity assertion follows directly from the definition of $H^\sigma_p(C)$ and Lemma 4.1. □

Finite segment limitation. If $p(C) = X$ is a proper bounded interval, the global equality above is not asserted for the unrestricted real line spaces V_j. A finite segment approximation theorem requires boundary-adapted spaces or an explicitly specified extension operator. The bounded segment in Section 5 is therefore used only for the numerical verification of the arc length discretization.

5. Numerical experiment and symbolic mask examples

The numerical test first verifies the Euler approximation of the reference arc length map on a bounded injective segment. The parameters are

$$a = 2, \qquad b = 1.2, \qquad v_0 = 0.3, \qquad \Omega = 2, \qquad I = [0, \pi/2].$$

The parametrization γ is injective on this interval because its first coordinate

$$x(t) = (2 + 0.3\cos 2t)\cos t$$

satisfies

$$x'(t) = -0.6\sin(2t)\cos t - (2 + 0.3\cos 2t)\sin t < 0, \qquad 0 < t \le \pi/2.$$

The arc length map is computed with $N = 2000$ left-endpoint Euler steps. A composite trapezoidal rule with 200,000 subintervals is used as the reference. The resulting reference length is $s(\pi/2) = 2.826077357655$, and the maximum absolute arc length coordinate error at the Euler nodes is 1.11×10^{-4}. The grid refinement results in Table 1 show the expected first-order decay of this error.

Table 1. Grid refinement check for the left-endpoint Euler arc length approximation.

N	$\max_i \lvert s_N(t_i) - s_{\mathrm{ref}}(t_i)\rvert$	Observed order
250	8.85870×10^{-4}	–
500	4.42940×10^{-4}	0.99998
1000	2.21470×10^{-4}	1.00000
2000	1.10735×10^{-4}	1.00000

The inverse projection is also checked numerically. At every Euler node, let

$$t_i^{\mathrm{rec}} = s_{\mathrm{ref}}^{-1}(s_N(t_i)), \qquad E_{\mathrm{rec}} = \max_i \|\gamma(t_i) - \gamma(t_i^{\mathrm{rec}})\|_2.$$

Piecewise linear interpolation of the dense reference inverse gives $E_{\mathrm{rec}} = 1.11 \times 10^{-4}$. This is the reconstruction error of the curve map $\gamma \circ s_{\mathrm{ref}}^{-1} \circ s_N$ relative to γ at the Euler nodes; the reference inverse is used so that the forward Euler discretization error is not cancelled by reusing the same discrete inverse.

Because the two symbolic mask examples below do not independently establish the existence of an L^2-stable scaling generator, no wavelet signal reconstruction error is reported. In this numerical subsection, "reconstruction error" refers only to the geometric inverse projection error E_{rec} defined above.

For the two-direction mask in Example 5.2, define the real line structured symbol matrix explicitly by

$$\mathcal{M}(\eta) = \begin{bmatrix} P^+(\eta) & P^-(\eta) \\ P^-(-\eta) & P^+(-\eta) \end{bmatrix},$$

which is the matrix used in Proposition 4.1. On the grid $\eta_m = -\pi + 2\pi m/8192$, $m = 0, \ldots, 8192$, the paraunitary mask identity residual is defined by

$$R_{\mathrm{PM}} = \max_{0 \le m \le 8192} \|\mathcal{M}(\eta_m)\mathcal{M}(\eta_m)^* + \mathcal{M}(\eta_m + \pi)\mathcal{M}(\eta_m + \pi)^* - I_2\|_2\,, \tag{5.1}$$

where $\|\cdot\|_2$ is the spectral matrix norm. IEEE double-precision evaluation gives $R_{\mathrm{PM}} = 1.67 \times 10^{-15}$, which is at roundoff level. The eigenvalues of $\mathcal{M}(0)$ are 1 and $7/20 - \sqrt{31}/10 \approx -0.2067764363$, so the mask matrix spectral condition is also satisfied. The reproducibility parameters and numerical error indicators are summarized in Table 2. The finite segment test shown in Figure 1 concerns only the discretized arc length map on an embedded spatial branch.

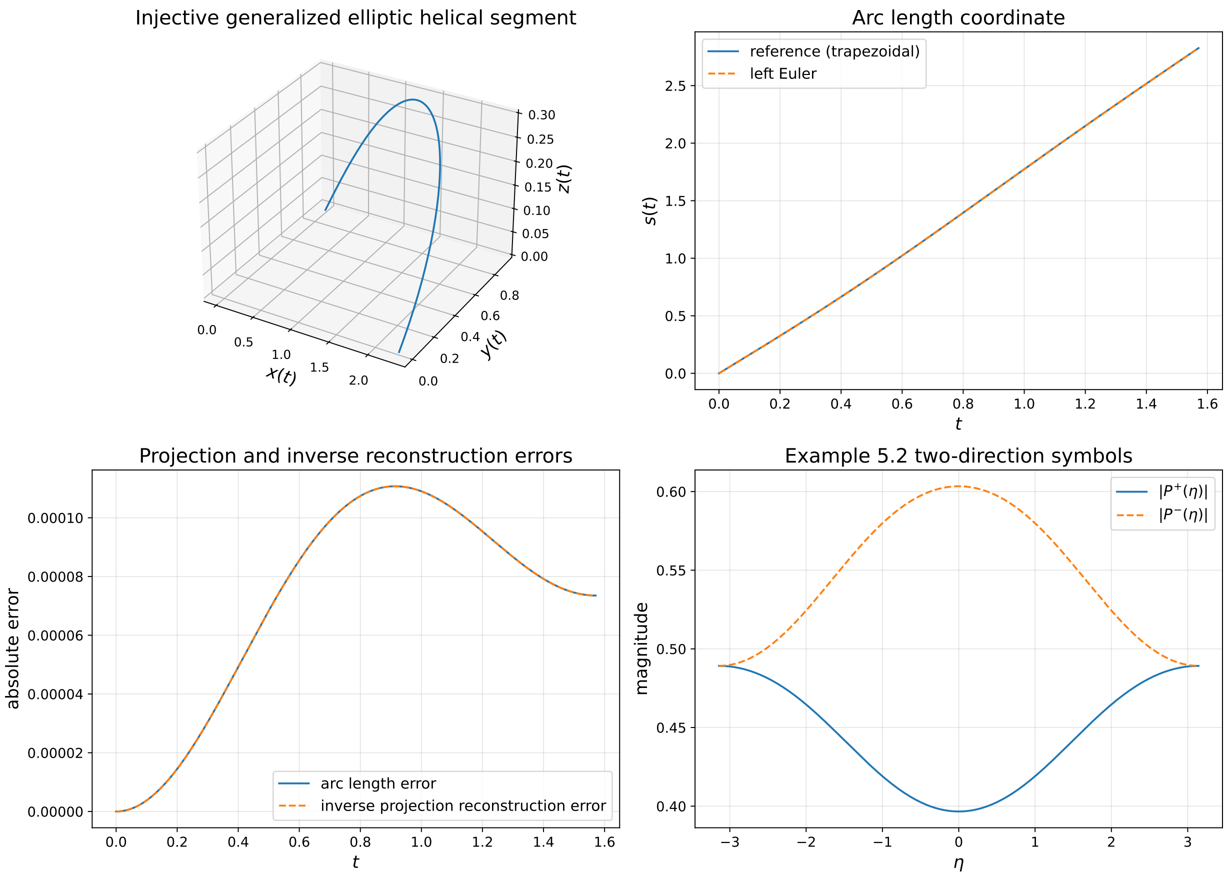

Figure 1. Reproducible numerical test on the injective segment $I = [0, \pi/2]$: the generalized elliptic helical curve, the reference and Euler arc length coordinates, the arc length and inverse projection errors, and the magnitudes of the two-direction symbols used in Example 5.2.

Table 2. Reproducibility parameters and numerical error indicators.

Quantity	Value
Curve parameters	$a = 2$, $b = 1.2$, $v_0 = 0.3$, $\Omega = 2$
Parameter interval	$[0, \pi/2]$
Euler steps	$N = 2000$
Reference trapezoidal subintervals	200000
Reference arc length	2.826077357655
Maximum arc length error	1.11×10^{-4}
Frequency grid	8193 points on $[-\pi, \pi]$
Geometric inverse projection reconstruction error	1.11×10^{-4}
Paraunitary mask identity residual ($\|\cdot\|_2$)	1.67×10^{-15}
Eigenvalues of $\mathcal{M}(0)$	1 and $\frac{7}{20} - \frac{\sqrt{31}}{10} \approx -0.2067764363$

The two symbolic refinement examples below are interpreted on the global parametrized carrier C_γ with $I = \mathbb{R}$, for which $p(C_\gamma) = \mathbb{R}$ by (2.9).

Example 5.1. Consider the following two-direction mask on the global parametrized carrier $C = C_\gamma$ of a generalized elliptic helical curve with $I = \mathbb{R}$ and $p(C) = \mathbb{R}$. Choose $M = L = 2$, and

$$S^+(\eta) = \frac{3}{4}, \qquad S^-(\eta) = \frac{1}{4}.$$

Then, $s_0^+ = 3/4 \geq 0$, $s_0^- = 1/4 \geq 0$, $S^+(0) + S^-(0) = 1$, and

$$S^+(\pi) + e^{-i2\pi} S^-(\pi) = 1 \neq 0.$$

These calculations verify the factorization, non-negativity, normalization, and nonvanishing conditions displayed in Lemma 4.1. The two symbols are

$$P^{C,+}(\eta) = \frac{3}{4}\left(\frac{1 + e^{-i\eta}}{2}\right)^2,$$
$$P^{C,-}(\eta) = \frac{1}{4}\left(\frac{1 + e^{-i\eta}}{2}\right)^2.$$

Because $P^{\pm}(\eta) = \frac{1}{2}\sum_k p_k^{\pm} e^{-ik\eta}$, the refinement coefficients are

$$(p_0^+, p_1^+, p_2^+) = \left(\frac{3}{8}, \frac{3}{4}, \frac{3}{8}\right), \qquad (p_0^-, p_1^-, p_2^-) = \left(\frac{1}{8}, \frac{1}{4}, \frac{1}{8}\right).$$

The coefficient sums are

$$\sum_k p_k^+ = \frac{3}{2}, \qquad \sum_k p_k^- = \frac{1}{2},$$

and therefore,

$$\sum_k p_k^+ + \sum_k p_k^- = 2, \qquad \left|\sum_k p_k^+ - \sum_k p_k^-\right| = 1 < 2.$$

Consequently, the alternative (IV) of Theorem 2 in [15] with dilation factor $m = 2$ applies: In the normalization used there, the associated real line refinement equation has a unique compactly supported distributional solution ϕ. Moreover, the masks satisfy the non-negative factorization hypotheses of Theorem 11 in [15]. Hence, this solution belongs to $L^2(\mathbb{R})$, has polynomial reproduction approximation order 2 in the sense of Definition 3 of [15], and has Sobolev regularity at least $3/2$; in the nonendpoint convention adopted in this paper,

$$\phi \in H^{\sigma}(\mathbb{R}) \qquad \text{for every real } 0 \leq \sigma < \frac{3}{2}.$$

The curve function $\phi^C = \phi \circ p$ is therefore a well-defined compactly supported $L^2(C)$ refinable solution, and coefficient transport gives

$$\begin{aligned} \phi^C(\xi) = {} & \frac{3}{8}(\phi^C \circ p^{-1})(2p(\xi)) + \frac{3}{4}(\phi^C \circ p^{-1})(2p(\xi) - 1) + \frac{3}{8}(\phi^C \circ p^{-1})(2p(\xi) - 2) \\ & + \frac{1}{8}(\phi^C \circ p^{-1})(-2p(\xi)) + \frac{1}{4}(\phi^C \circ p^{-1})(1 - 2p(\xi)) + \frac{1}{8}(\phi^C \circ p^{-1})(2 - 2p(\xi)). \end{aligned} \tag{5.2}$$

By unitarity, the L^2 property, polynomial reproduction in the arc length variable, and the nonendpoint regularity conclusion transfer to the carrier; in particular,

$$\phi^C \in H^{\sigma}_p(C) \qquad \text{for every real } 0 \leq \sigma < \frac{3}{2}.$$

If, in addition, the associated real line spaces satisfy the independent Jackson estimate (4.5) with $n = 2$, then Theorem 4.2 transfers Sobolev best approximation order 2 to the curve spaces. The existence and L^2 conclusions above do not by themselves imply the Riesz basis property, an orthogonal multiresolution analysis, or orthogonality; those properties still require their respective independent hypotheses.

Example 5.2. Example 5.1 of Keinert and Kwon [26] motivates the support locations and algebraic form used here. The coefficients below are a rescaled mask formulated specifically for the normalization of the present paper; they are not claimed to be a term-by-term rewriting of the coefficients in that source. In the present notation,

$$P^{\pm}(\eta) = \frac{1}{2} \sum_{k \in \mathbb{Z}} p^{\pm}_k e^{-ik\eta}.$$

No orthogonality, spectral, existence, stability, or approximation order property is inferred solely from [26]; the algebraic properties claimed below are verified independently in the present normalization. The nonzero coefficients are

$$\begin{aligned} & p^+_1 = \frac{93 - 13\sqrt{31}}{320}, \quad p^+_2 = \frac{341 - 11\sqrt{31}}{320}, \quad p^+_3 = \frac{11 - 11\sqrt{31}}{320}, \quad p^+_4 = \frac{-13 + 3\sqrt{31}}{320}, \\ & p^-_4 = \frac{-31 + \sqrt{31}}{320}, \quad p^-_5 = \frac{217 + 23\sqrt{31}}{320}, \quad p^-_6 = \frac{23 + 7\sqrt{31}}{320}, \quad p^-_7 = \frac{-1 + \sqrt{31}}{320}. \end{aligned} \tag{5.3}$$

Thus,

$$P^+(\eta) = \frac{1}{2} \sum_{k=1}^{4} p^+_k e^{-ik\eta}, \qquad P^-(\eta) = \frac{1}{2} \sum_{k=4}^{7} p^-_k e^{-ik\eta}.$$

Direct expansion gives

$$\mathcal{M}(\eta)\mathcal{M}(\eta)^* + \mathcal{M}(\eta+\pi)\mathcal{M}(\eta+\pi)^* = I_2,$$

with $\mathcal{M}$ defined in Proposition 4.1. Moreover,

$$\mathcal{M}(0) = \begin{bmatrix} \frac{27}{40} - \frac{\sqrt{31}}{20} & \frac{13}{40} + \frac{\sqrt{31}}{20} \\ \frac{13}{40} + \frac{\sqrt{31}}{20} & \frac{27}{40} - \frac{\sqrt{31}}{20} \end{bmatrix}$$

has eigenvalues 1 and $\frac{7}{20} - \frac{\sqrt{31}}{10} \approx -0.2067764363$. Hence, the paraunitary mask identity and the mask matrix spectral condition are both satisfied for this mask. Because the row sum eigenvalue equals 1, this mask lies in the normalization-compatible second branch of Theorem 3.2. These exact calculations verify the coefficients, exponent signs, Hermitian algebraic orthogonality condition, and spectral condition in the normalization used here. These calculations do not establish the existence or uniqueness of a compactly supported distributional solution, convergence of the infinite matrix product, or the existence of an L^2-stable scaling generator. Any distributional solvability conclusion must be obtained from a separate applicable existence theorem after all of its hypotheses have been verified. If a normalized L^2-stable real line refinable generator with the required Riesz basis exists, Proposition 4.1 shows only that its mask passes the necessary Hermitian test. Orthogonality still requires an additional independent sufficiency argument; if orthogonality is established separately, Theorem 3.1 transports the generator and its Riesz structure to the curve, and unitarity transports the established orthogonality. No approximation order claim is made for this example; the conditional order-2 illustration is Example 5.1. If a corresponding curve scaling function ϕ^C exists under the stated solvability and stability hypotheses, its associated formal refinement relation on the carrier is

$$\phi^C(\xi) = \sum_{k=1}^{4} p_k^+ (\phi^C \circ p^{-1})(2p(\xi) - k) + \sum_{k=4}^{7} p_k^- (\phi^C \circ p^{-1})(k - 2p(\xi)), \tag{5.4}$$

where the coefficients are exactly those in (5.3). This example provides a full algebraic check of the signs, exponent indices, the mask matrix spectral condition, and the Hermitian paraunitary mask identity. The mask matrix spectral condition alone does not establish the existence or uniqueness of a compactly supported distributional solution. Such a conclusion requires a separate applicable existence theorem with all hypotheses verified; the existence of an L^2-stable scaling generator remains conditional on the separate stability and convergence hypotheses stated above. Any orthogonality conclusion additionally requires an independently verified sufficiency hypothesis or a direct orthogonality proof.

6. Conclusions

In this paper, two-direction scaling functions on generalized elliptic helical curves were investigated through an arc length-preserving projection. The spatial trace was distinguished from the parametrized carrier. On the global carrier with $I = \mathbb{R}$, the positive speed lower bound implies $p(C) = \mathbb{R}$, even when the spatial trace is periodic or self-intersecting; repeated spatial locations remain distinct because their parameter labels are retained. The Euler method was tested separately on a bounded injective spatial segment. The projection was then used to transport the two-direction multiresolution framework and the corresponding refinement equations from the real line arc length coordinate to the carrier.

Furthermore, the relationship between the refinement coefficients on the real line and those on generalized elliptic helical curves was analyzed. On this basis, the necessary Hermitian orthogonality conditions and the approximation order properties were examined. A structured Hermitian matrix mask screening condition was also formulated for an already existing normalized L^2-stable two-direction scaling generator satisfying the stated Riesz basis assumptions; no sufficiency conclusion was drawn without an additional independent hypothesis. Finally, a reproducible Euler projection test on an injective segment and two algebraically checked symbolic examples were provided.

The results show that the parameter restrictions $a > 0$, $b > 0$, $|v_0| < \min\{a, b\}$ yield a positive global speed lower bound. Therefore, the arc length coordinate maps the global parametrized carrier over $I = \mathbb{R}$ homeomorphically onto $\mathbb{R}$. On every subinterval on which γ is a topological embedding—in particular, on every compact interval on which γ is injective—the corresponding carrier segment is homeomorphic to, and may be identified with, the embedded spatial branch; at a self-intersection, the global carrier retains the branch label and avoids a multivalued inverse. In this precise sense, arc length-preserving projection provides a rigorous way to transfer two-direction wavelet analysis from the real line to generalized elliptic helical parametrized curves.

The numerical section validates only the discretized arc length map on one injective segment and checks the stated mask identities. It does not test aircraft, satellite, biological, seismic, financial, or other application data, and no empirical claim for those settings is made.

Author contributions

Gang Wang and Zhihui Zhang: Conceptualization, methodology, formal analysis, investigation, validation, supervision, writing–original draft, and writing–review and editing. Both authors jointly contributed to all aspects of the work and have read and approved the submitted version of the manuscript.

Use of Generative-AI tools declaration

The authors declare they have not used Artificial Intelligence (AI) tools in the creation of this article.

Conflict of interest

The authors declare no conflicts of interest.

References

1. I. Daubechies, *Ten lectures on wavelets*, Philadelphia: Society for Industrial and Applied Mathematics, 1992. https://doi.org/10.1137/1.9781611970104
2. X. Zhou, B. Wang, Wavelet analysis on some smooth surface with nonzero constant Gaussian curvature, *Int. J. Wavelets Multi.*, **16** (2018), 1850007. https://doi.org/10.1142/S0219691318500078

3. D. Zhang, X. You, P. Wang, S. N. Yanushkevich, Y. Y. Tang, Facial biometrics using nontensor product wavelet and 2D discriminant techniques, *Int. J. Pattern Recognit. Artif. Intell.*, **23** (2009), 521–543. https://doi.org/10.1142/S0218001409007260
4. F. In, S. Kim, *An introduction to wavelet theory in finance: A wavelet multiscale approach*, Singapore: World Scientific, 2012. https://doi.org/10.1142/8431
5. X. Zhou, Wavelet transform on regression trend curve and its application in financial data, *Int. J. Wavelets Multi.*, **18** (2020), 2050040. https://doi.org/10.1142/S021969132050040X
6. X. Zhou, G. Wang, Biorthogonal wavelet on a logarithm curve $\mathbb{C}$, *J. Math.*, **2021** (2021), 7985069. https://doi.org/10.1155/2021/7985069
7. F. Mujica, J. P. Leduc, M. J. T. Smith, R. Murenzi, SpatioTemporal wavelets: A group-theoretic construction for motion estimation and tracking, *SIAM J. Appl. Math.*, **61** (2000), 596–632. https://doi.org/10.1137/S0036139999351864
8. J. P. Leduc, Spatio-temporal wavelet transforms for digital signal analysis, *Signal Process.*, **60** (1997), 23–41. https://doi.org/10.1016/S0165-1684(97)84221-1
9. J. P. Antoine, D. Rosca, P. Vandergheynst, Wavelet transform on manifolds: Old and new approaches, *Appl. Comput. Harmon. Anal.*, **28** (2010), 189–202. https://doi.org/10.1016/j.acha.2009.10.002
10. D. Rosca, Wavelet analysis on some surfaces of revolution via area preserving projection, *Appl. Comput. Harmon. Anal.*, **30** (2011), 262–272. https://doi.org/10.1016/j.acha.2010.09.008
11. B. Q. Wang, G. Wang, X. H. Zhou, Y. Su, Wavelet analysis on developable surface base on area preserving projection, *Int. J. Wavelets Multi.*, **13** (2015), 1550007. https://doi.org/10.1142/S0219691315500071
12. B. Q. Wang, G. Wang, X. H. Zhou, A local wavelet transform on the torus T^2, *Int. J. Wavelets Multiresolut. Inf. Process.*, **13** (2015), 1550027. https://doi.org/10.1142/S0219691315500277
13. X. Zhou, Wavelet analysis on a generalized helix space curves and its examples, *EURASIP J. Adv. Signal Process.*, **2024** (2024), 70. https://doi.org/10.1186/s13634-024-01164-w
14. B. Wang, G. Wang, X. Zhou, Construction of the multi-wavelets on some smooth plane curves via length-preserving projection, *Int. J. Wavelets Multi.*, **12** (2014), 1450005. https://doi.org/10.1142/S0219691314500052
15. S. Z. Yang, Y. F. Li, Two-direction refinable functions and two-direction wavelets with high approximation order and regularity, *Sci. China Ser. A Math.*, **50** (2007), 1687–1704. https://doi.org/10.1007/s11425-007-0091-7
16. R. R. Coifman, M. Maggioni, Diffusion wavelets, *Appl. Comput. Harmon. Anal.*, **21** (2006), 53–94. https://doi.org/10.1016/j.acha.2006.04.004
17. D. K. Hammond, P. Vandergheynst, R. Gribonval, Wavelets on graphs via spectral graph theory, *Appl. Comput. Harmon. Anal.*, **30** (2011), 129–150. https://doi.org/10.1016/j.acha.2010.04.005
18. D. I. Shuman, S. K. Narang, P. Frossard, A. Ortega, P. Vandergheynst, The emerging field of signal processing on graphs: Extending high-dimensional data analysis to networks and other irregular domains, *IEEE Signal Process. Mag.*, **30** (2013), 83–98. https://doi.org/10.1109/MSP.2012.2235192

19. S. Mallat, Group invariant scattering, *Commun. Pure Appl. Math.*, **65** (2012), 1331–1398. https://doi.org/10.1002/cpa.21413

20. M. Perlmutter, F. Gao, G. Wolf, M. Hirn, Geometric wavelet scattering networks on compact Riemannian manifolds, In: Proceedings of the First Mathematical and Scientific Machine Learning Conference, *Proc. Mach. Learn. Res.*, **107** (2020), 570–604. Available from: `https://proceedings.mlr.press/v107/perlmutter20a.html`.

21. F. Gama, E. Isufi, G. Leus, A. Ribeiro, Graphs, convolutions, and neural networks: From graph filters to graph neural networks, *IEEE Signal Proc. Mag.*, **37** (2020), 128–138. https://doi.org/10.1109/MSP.2020.3016143

22. M. Defferrard, X. Bresson, P. Vandergheynst, Convolutional neural networks on graphs with fast localized spectral filtering, *Adv. Neural Inform. Proc. Syst. 29*, Red Hook: Curran Associates, 2016, 3844–3852. Available from: `https://proceedings.neurips.cc/paper/2016/hash/04df4d434d481c5bb723be1b6df1ee65-Abstract.html`.

23. B. Xu, H. Shen, Q. Cao, Y. Qiu, X. Cheng, *Graph wavelet neural network*, Proceedings of the International Conference on Learning Representations, New Orleans, USA, 2019. Available from: `https://openreview.net/forum?id=H1ewdiR5tQ`.

24. M. M. Bronstein, J. Bruna, T. Cohen, P. Veličković, Geometric deep learning: Grids, groups, graphs, geodesics, and gauges, *arXiv*, 2021. https://doi.org/10.48550/arXiv.2104.13478

25. X. Zhou, The equation and figures of a class of generalized helicoid, *J. Suzhou Univ.*, **31** (2016), 93–95 (in Chinese).

26. F. Keinert, S. G. Kwon, Point values and normalization of two-direction multiwavelets and their derivatives, *Kyungpook Math. J.*, **55** (2015), 1053–1067. https://doi.org/10.5666/KMJ.2015.55.4.1053

AIMS Press